Chapter 2

An Interest in Thiolate Coordination and Hydrogen Bonding

Parts reproduced with permission from Whited, C. A., W. Belliston-Bittner, A. R. Dunn, J. R. Winkler, H. B. Gray. Nanosecond photoreduction of inducible nitric oxide synthase by a Ru-diimine electron tunneling wire bound distant from the active site. *J. Inorg. Biochem*. 2009; *103*: 906–911.

2.1 Abstract

The Gray group has been studying electron transfer in protein systems for the past three decades. During this time a vast amount of information has been collected concerning the nature of the protein matrix and its ability to facilitate such charge transfer reactions. This led to the development of techniques for the covalent attachment of photosensitizers to metalloproteins, and later to the development of compounds consisting of sensitizers linked to substrates (dubbed "wires") in order to promote interactions between the photosensitizer and the metal active site buried deep within the protein. A Ru-diimine wire, $[(4,4',5,5'\text{-tetramethylbipyridine})_2Ru(F_9bp)]^{2+}$ (tmRu-F_9bp, where F_9bp is 4-methyl-4'-methylperfluorobiphenylbipyridine), binds tightly to the oxidase domain of inducible nitric oxide synthase (iNOSoxy). The binding of tmRu-F_9bp is independent of tetrahydrobiopterin, arginine, and imidazole, indicating that the wire resides on the surface of the enzyme, distant from the active-site heme. Photoreduction of an imidazole-bound active-site heme iron in the enzyme-wire conjugate ($k_{ET} = 2(1) \times 10^7$ s^{-1}) is fully seven orders of magnitude faster than the *in vivo* process. Wires such as this surface-binding example are used to study the various electron transfer processes in metalloenzymes in an effort to generate and characterize reactive intermediate species that are otherwise unobservable.

2.2 Introduction

Electron Transfer in Metalloproteins

All life on our planet must carefully balance both electrons and protons as well as defend itself against oxidative damage caused by our highly oxidizing atmosphere. Processes necessary for human life, such as respiration, require a complex system of proteins and enzymes in order to harness the energy in oxygen in a useful way without causing damage to an organism through Fenton chemistry and the like.[1] The two following reactions (**Scheme 2.1**) have been called the most important reactions on the planet (Harry Gray, countless presentations and informal conversations). These are photosynthesis (in part) and aerobic respiration.

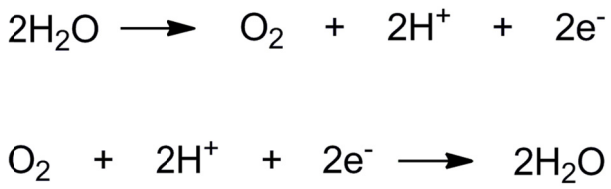

Scheme 2.1. The two most important reactions on our planet: photosynthesis (top) and aerobic respiration (bottom).

In plants and photosynthetic bacteria, photosynthesis is the process of harnessing energy from sunlight to convert carbon monoxide into higher, more complex C_n-containing molecules necessary for the health of the organism.[2] Along the way water is oxidized, which produces dioxygen as a high-energy by-product. It is this oxygen that most higher life forms on this planet breathe in for the process of respiration, releasing the energy of dixoygen and producing water.

Protons and electrons must be finely controlled and delivered just when necessary in order to achieve the desired reactivity in each of these two processes and sustain life.

Electron transfers occur from one redox active compound to another. In biological systems these are commonly flavins, quinones, porphyrins, and metal centers. Nature developed protein scaffolds in order to insulate these redox sites from one another, preventing deleterious side reactions and promoting only the specific reaction of choice. The very nature of these protein scaffolds is designed to inhibit the random transfer of charge, making electron transfer difficult. The physical presence of the scaffold separates the two species participating in electron transfer. Without these scaffolds, species would simply move toward the thermodynamically favored state and cells would stop functioning. Particular reactions are desired, however, and therefore the protein must somehow also facilitate these vital charge transfers over large distances (sometimes greater than 20 Å). The Gray group has long been interested in understanding how proteins mediate these long-range electron transfer reactions.

A very powerful theory for studying and understanding electron transfer (ET) reactions has been developed by the Caltech professor Rudy Marcus. While, originally developed with simpler systems in mind, this theoretical formalism has proven applicable in protein systems and provides a context within which ET in metalloproteins can be studied.

Semi-Classical Marcus Theory

Marcus Theory is a formalism through which electron transfer reactions can be understood.[3-4] It relies on the Franck-Condon Principal which states that when a molecule absorbs a photon the rearrangement of electrons is nearly instantaneous (occurs over the femtosecond timescale).[4] However, the nuclei of the constituent atoms are much heavier than the electrons and, therefore, nuclear movement is incredibly slow on the timescale of

moving electrons. This nearly always results in positioning the molecule in a vibrational excited state within the new electronic state. Nonradiative decay allows the molecule to relax to the lowest vibrational state within the excited electronic state before releasing the energy as a photon (the lifetime of vibrational excited states are nearly always shorter than the lifetimes of electronic excited states). Finally, the molecule luminesces to return to its ground state, but the photon released is of lower energy than the originally absorbed photon (the difference being the energy of the vibrational states).

In Marcus Theory, the Franck-Condon Principle is applied to electronic states of both the donor molecule (D) and the acceptor (A). Each state can be represented by a parabola (**Figure 2.1**). In the case of much of the Gray group's work, the donor and acceptor are linked by a bridging moiety, B, through which the electron is transferred.

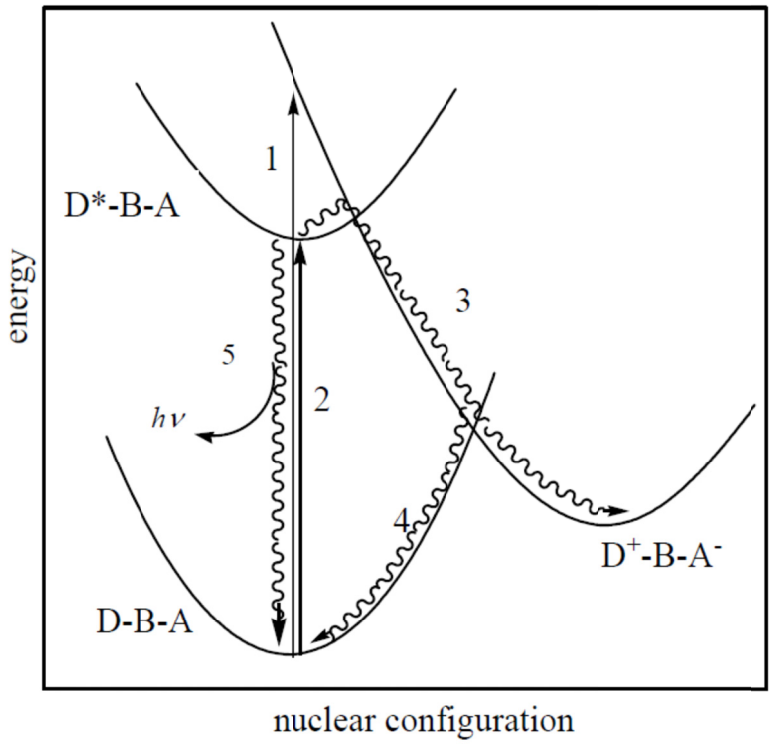

Figure 2.1. Electronic states of a representative D-B-A molecule.

First, a photon is absorbed, promoting the donor to its excited state. From this state it can either relax to the ground state through both radiative and non-radiative decay, or its excited electron can be transferred to the acceptor molecule. The Franck-Condon Principle requires that the nuclei, which remain fixed on the timescale of electronic movement, be in a configuration corresponding to the product complex, in other words the transition state lies at a point where the reactants and products have the same nuclear configuration (the point where two parabolas cross in **Figure 2.1**). From this requirement, a relationship between the rate of such a reaction and its driving force can be extrapolated.

In proteins in particular, electronic coupling between the donor and acceptor can often be quite weak. Metal centers are buried within insulating protein scaffolds and separated by tens of Ångstroms. The probability of transferring an electron is therefore quite low each time the nuclei form the transition state, meaning it must be formed and reformed many times before the desired reaction occurs. This places such reactions in the nonadiabatic limit. Semiclassical Marcus Theory predicts the following Equation 2.1 relating the rate of electron transfer to the driving force for the reaction (ΔG°), the electronic coupling between donor and acceptor (H_{AB}), and the reorganizational parameter (λ).

$$k_{ET} = \left(\frac{4\pi^3}{h^2 \lambda k_b T}\right)^{1/2} H_{AB}^2 \exp\left[\frac{-(\Delta G^o + \lambda)^2}{4\lambda k_b T}\right] \qquad (2.1)$$

The coupling constant, H_{AB}, is a function of the distance between donor and acceptor (as defined by the edge-to-edge distance) and another factor β, Equation 2.2. This second

term, β, describes how well the intervening medium facilitates electron transfer, vacuum being the poorest at promoting ET. The abilities of various media to promote electron transfer has been studied extensively by the Gray group over the past few decades, enabling the generation of Tunneling Timetables (Figure 2.2). For each medium the smaller the slope and the higher the line lies on the plot, the greater the rate of ET over a particular distance, meaning that particular medium transfer electrons better than other media with greater slopes. (Intuitively, conjugated bonds facilitate ET far better than vacuum.)

$$H_{AB} = H^{o}_{AB} \exp\left[-\beta\left(r_{AB} - r^{o}_{AB}\right)/2\right] \qquad (2.2)$$

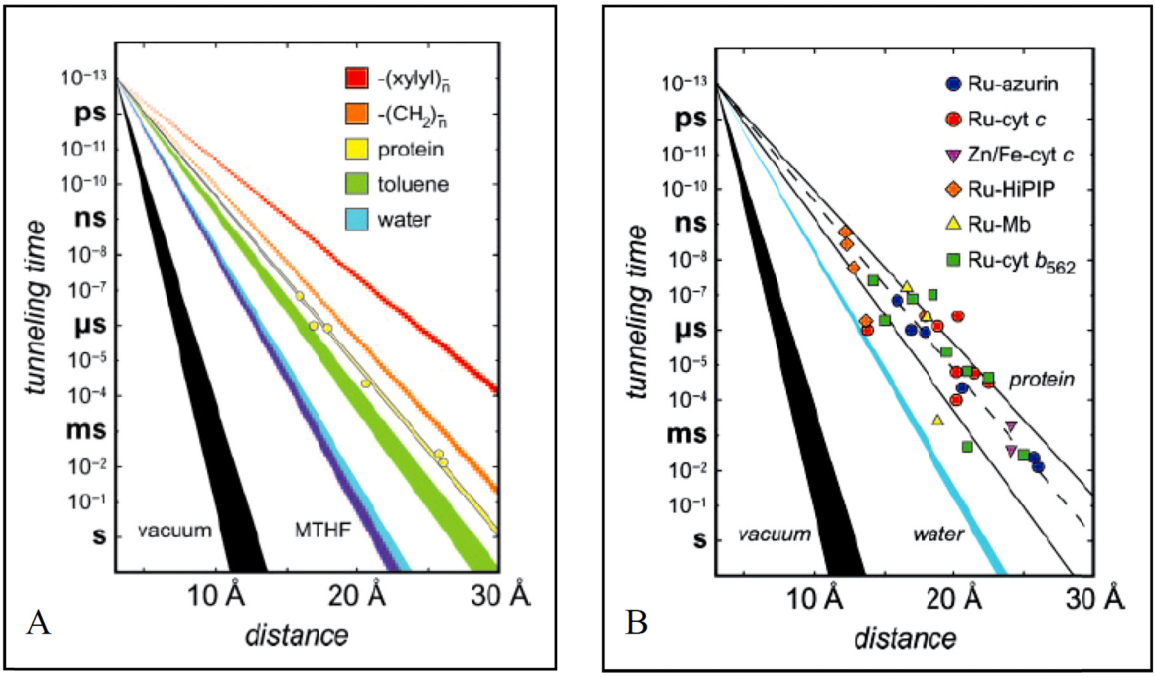

Figure 2.2. (A) Activationless electron Tunneling Timetable for various media: vacuum (black, β = 2.9–4.0 $Å^{-1}$), methyl-THF (violet, β = 1.57–1.65 $Å^{-1}$), toluene in glass form (green, β = 1.18–1.28 $Å^{-1}$), xylyl bridge (red, β = 0.76 $Å^{-1}$), alkane bridges (orange, β = 1.0 $Å^{-1}$), and β-strand bridges in ruthenium modified azurin (yellow, β = 1.1 $Å^{-1}$). (B) Tunneling Timetable for intraprotein ET in ruthenium-modified azurin (blue circles), cytochrome c (red circles), myoglobin (yellow triangles), cytochrome b_{562} (green squares), high-potential iron protein (orange diamonds), and for interprotein ET in Fe:Zn cytochrome c crystals (fuchsia triangles). Solid lines illustrate the tunneling pathway predictions for coupling along β-strands (β = 1.0 $Å^{-1}$), and α-helices (β = 1.3 $Å^{-1}$); dashed line illustrates a 1.1 $Å^{-1}$ distance decay for reference. Distance decay through water is shown as a cyan wedge, vacuum in black.

One interesting consequence of Marcus Theory is the prediction of the so-called inverted region.[5] Marcus Theory predicts that the rate of ET first increases with increasing driving force, as is intuitive. However, the rate constant reaches a maximum where the driving force is equal to the reorganization energy of the system. Beyond this point, the rate then actually decreases. The origin of this effect is shown in **Figure 2.3**.

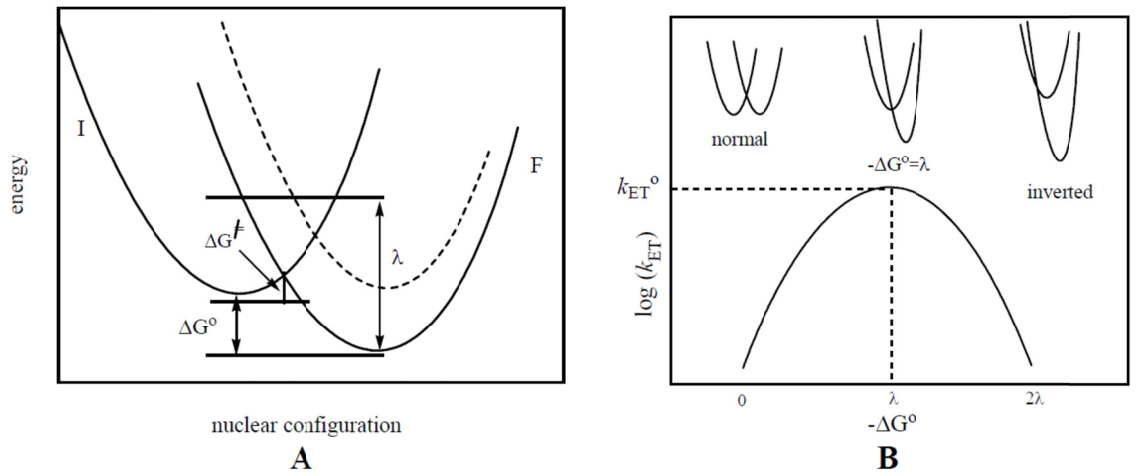

Figure 2.3. (A) Potential energy curves for an initial (I) and final (F) state, before and after ET, respectively. The dashed line represents that curve of the final state in a self-exchange reaction, where reactants and products are the same (isoergonic). (B) Rate of electron transfer as a function of increasing driving force showing the normal and inverted regions.

Flash/Quench Methodology

Excited states that have long lifetimes must be employed in order to study ET over the long distances often found in protein systems. The excited state of a Ru(II) tris-diimine complex is typically less than 1 μs. To increase this lifetime and thus increase the possibility of productive electron transfer, a flash/quench methodology was developed.[6] In this scheme another reactant is introduced, called a quencher (Q), which reacts with the excited state of the photosensitizer (Ru complex). A large excess of a small molecule quencher in solution can react quickly with the excited state of Ru(II), in effect quenching its excited state. Given the unique properties of Ru complexes, either oxidative or reductive quenchers can be used which will either oxidize or reduce the Ru to Ru(III) or Ru(I) (**Scheme 2.2**). This provides intermolecular charge separation and, in the absence of cage-trapped systems, greatly increases the length of time over which ET can occur. The new Ru species now lives on the order of milli- to microseconds, allowing for

the observation of much slower ET processes. This technique has been successfully used to study ET in many protein and enzyme systems.[7-9]

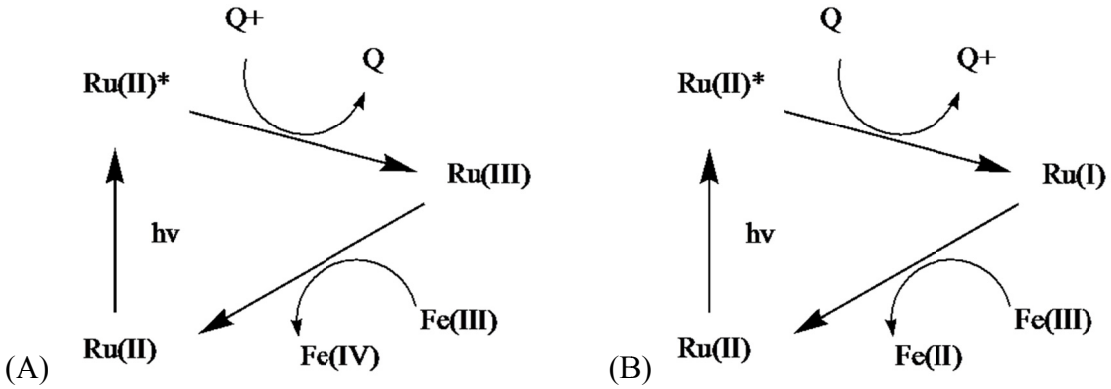

Scheme 2.2. Oxidative (A) and reductive (B) flash/quench schemes showing the production of highly reactive Ru complexes for ET reactions with a distant, buried protein active site (Fe as in a heme protein).

The Wires Project

A long-standing goal in our group is the development of methods to generate and observe high-valent iron-oxo complexes which are believed to play key roles as intermediates in the catalytic cycles of heme enzymes.[10-11] Direct observation during turnover would allow definitive identification of the active oxidant. Drawing on studies of similar enzymes and using techniques such as electron paramagnetic resonance spectroscopy under cryogenic conditions and X-ray crystallography, investigators have amassed a large body of evidence that strongly indicates that Compound I (**Scheme 2.3,** the ferryl P-IX racial cation shown in blue) is the active species.[12-14] The steps leading to formation of this highly reactive species are slow in comparison to the rate at which it reacts, making its observation problematic, as at best it is present in very low concentrations during catalysis.

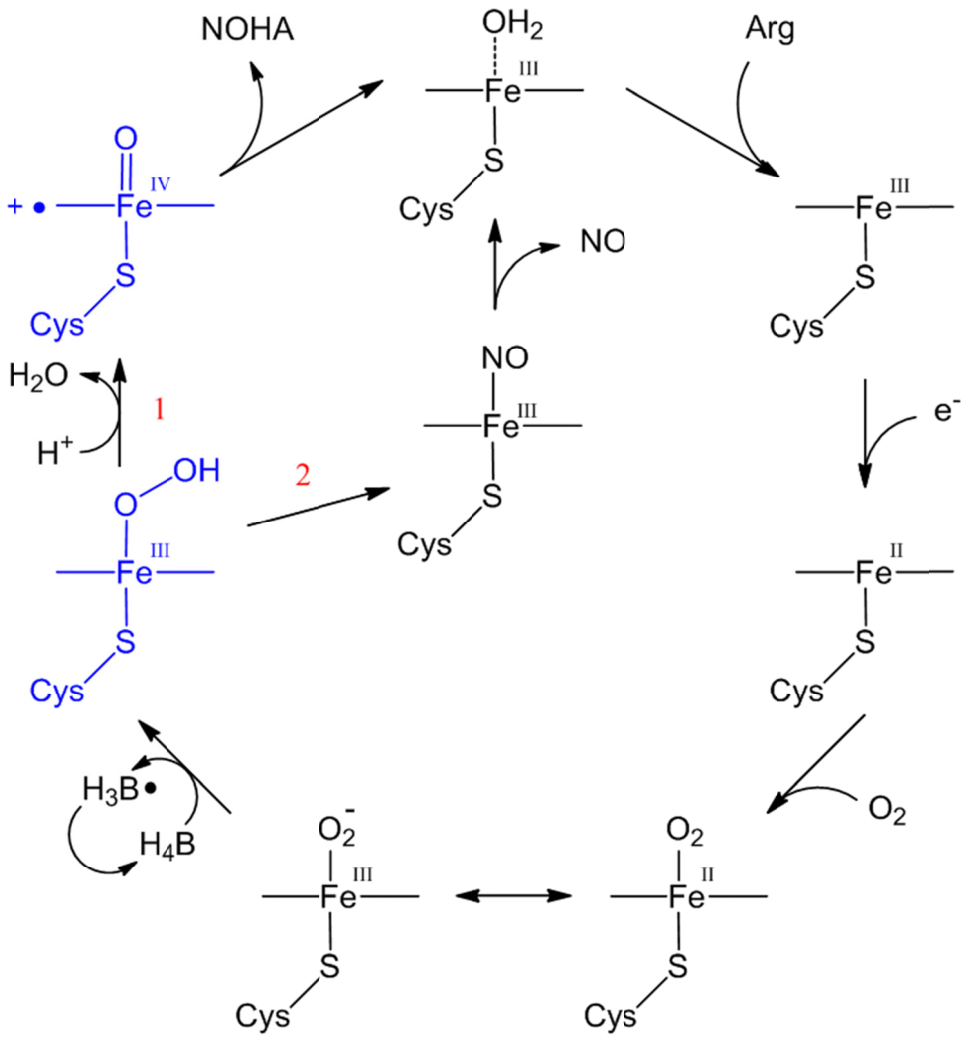

Scheme 2.3. Catalytic cycle of nitric oxide synthases, with putative intermediates highlighted in blue (as predicted by the cytochrome P450 mechanism). These putative intermediates are also the compounds of greatest interest. The numbers 1 and 2 (red) represent the path taken in the first and second turnovers.

We have investigated the redox photochemistry of two heme enzymes, microperoxidase-8 (MP-8, a heme octapeptide fragment of cytochrome *c*) and horseradish peroxidase (HRP).[7, 15] Visible excitation of $Ru(bpy)_3^{2+}$ (bpy is 2,2'-bipyridine) in the presence of oxidative quenchers in solution generates a powerful Ru(III)-diimine oxidant, which reacts rapidly with the heme to form the protoporphyrin-IX radical cation, which then oxidizes Fe(III) to give high-valent iron-oxo complexes of MP-8 and HRP. Attempts to generate high-valent hemes in P450s in reactions with

uncomplexed photogenerated oxidants were not successful so we changed course, as discussed in the following paragraphs.

Since 1999, we have developed sensitizer-linked electron tunneling wires that are able to deliver electrons and holes rapidly to and from deeply buried active sites of heme enzymes.[16] Attachment of the photosensitizer to the substrate promotes a close interaction between the two and increases the probability of electron transfer by increasing coupling (H_{AB}) (**Figure 2.4**). This technique proved very useful with cytochromes P450 and enabled the characterization of the enzyme in two states, open and closed as well as transient generation of a reduced state. These heavy-metal containing wires can actually promote crystallization of protein samples and provide a second transition metal besides the heme iron to aid in solving crystal structures. A selection of such molecules developed for the oxygenase domain of iNOS (iNOSoxy) is shown in **Table 2.1**.

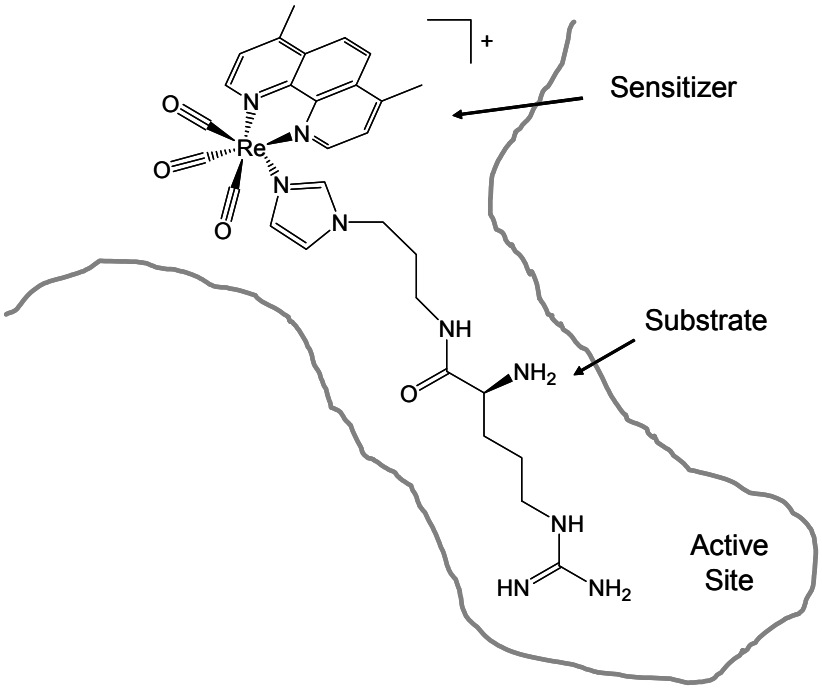

Figure 2.4: Substrates linked to sensitizers target active-site channels of enzymes.

Table 2.1: Ru(II) and Re(I) electron tunneling wires bind to iNOSoxy.

Channel-Binding Wires	
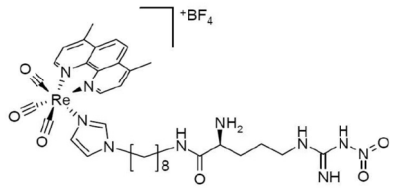 **1: *3 μM***	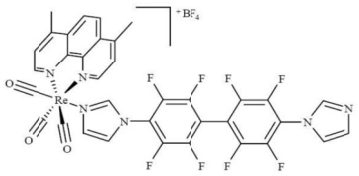 **5: *0.13 μM***
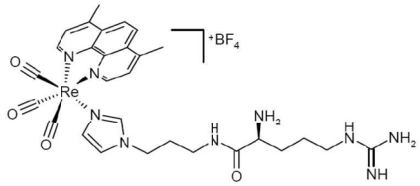 **2: *2 μM***	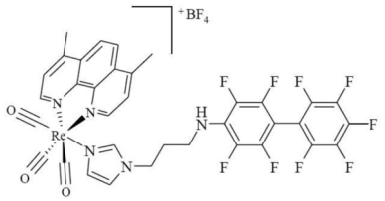 **6: *< 10 μM***
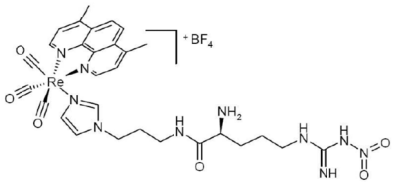 **3: *7 μM***	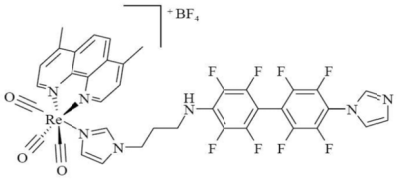 **7: *< 10 μM***
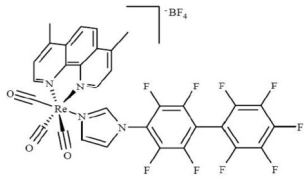 **4: *1.4 μM***	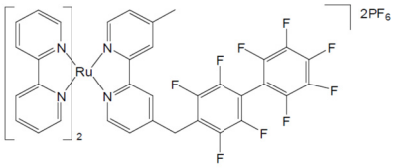 **8: *6.5 μM***

The dissociation constants of complexes that contain wires in the substrate channels of enzymes can be determined from analysis of shifts in Soret absorptions.[17] Examples of these shifts in the case of iNOSoxy are shown in **Figure 2.5**. The wires luminesce upon 355 nm (Re(I)) or 480 nm (Ru(II)) excitation. The emission overlap with heme absorptions triggers Förster energy transfer (FET), which accounts for the steady-state emission quenching observed upon binding of wires to iNOSoxy (**Figure 2.6**).

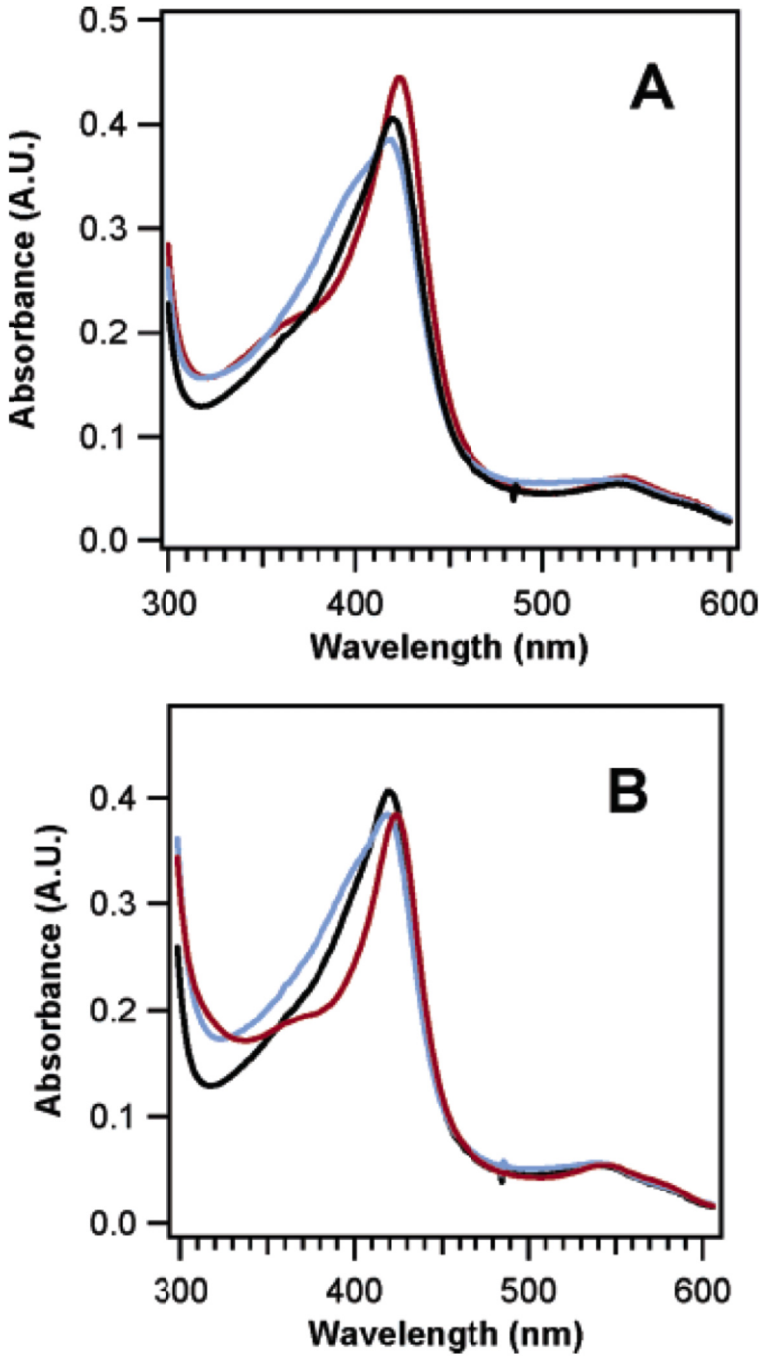

Figure 2.5: UV-visible absorption spectra of iNOSoxy: wire complexes. (A) iNOSoxy alone (5 μM; black) and bound to 1 equivalent each of **5** (red) and **4** (blue). (B) iNOSoxy alone (5 μM; black) and bound to 1 equivalent each of **7** (red) and **6** (blue).

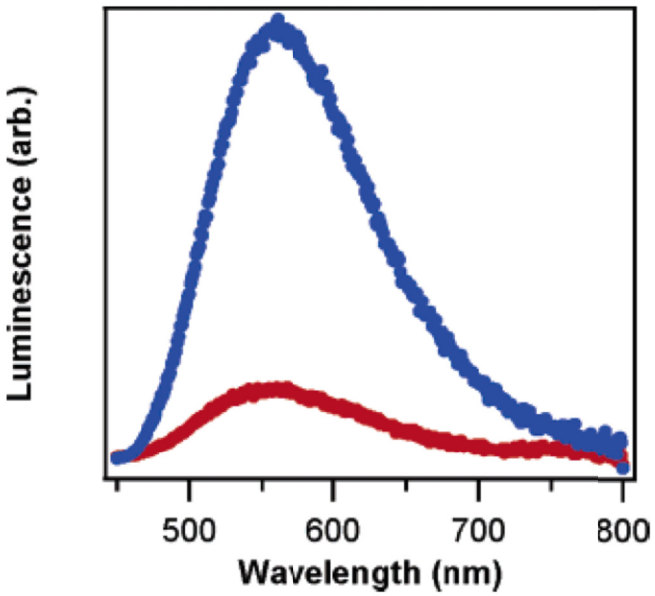

Figure 2.6: Steady-state luminescence spectra of **5** (2 μM; blue) and a 1:1 mixture of **5** and iNOSoxy (2 μM; red) with λ_{ex} = 355 nm.

Transient absorption measurements demonstrate that these wires reduce iNOSoxy upon 355 or 480 nm excitation. Reduction is indicated by a bleach near 420 nm, corresponding to the disappearance of the six-coordinate Fe(III) resting state and the formation of a new species (with absorption near 445 nm) assigned to six-coordinate Fe(II). Difference spectra were constructed from single-wavelength transient absorption traces 80 ns after excitation of the protein-bound wire **7** (**Figure 2.7**, blue) and 3 μs after excitation of protein-bound wire **5** (**Figure 2.7**, red).

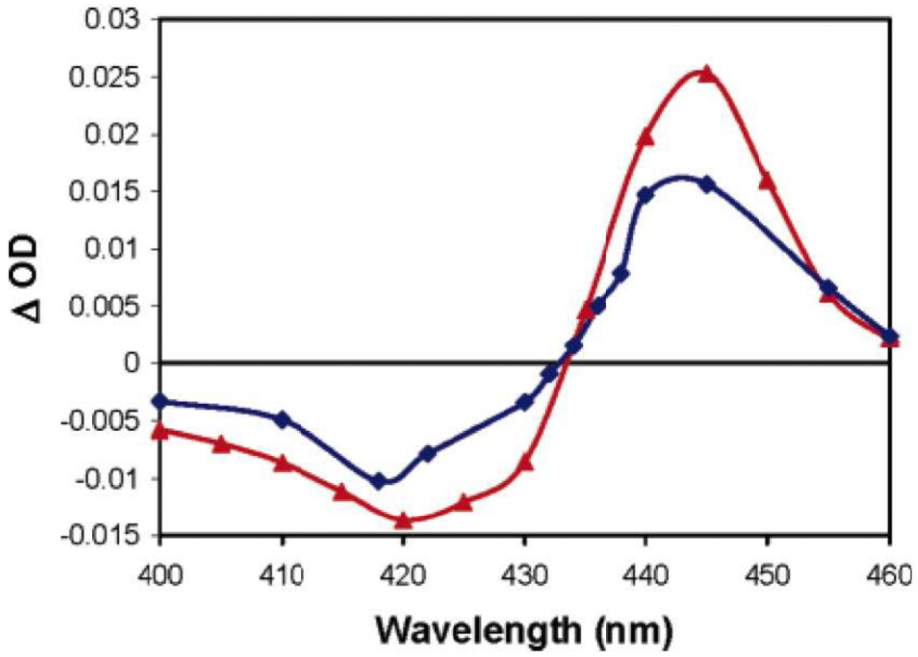

Figure 2.7. Difference spectra of a 1:1 mixture of **7** and iNOSoxy (5 μM, 80 ns after 355 nm excitation, blue squares) and a 1:1 mixture of **5** and iNOSoxy (11 μM, 3 μs after 355 nm excitation, red triangles) showing a bleach of a six-coordinate Fe(III) Soret (420 nm) and the appearance of a six-coordinate Fe(II) Soret (445 nm). Individual points were taken from single-wavelength transient absorption traces.

Picosecond transient absorption measurements demonstrate rapid formation of Fe(II) in the presence of wires **5** and **7**. By pumping with 70 ps, 355 nm pulses and probing with 442 nm radiation from a continuous wave He:Cd laser, we obtained transient absorbance traces that document the formation of a ferrous heme on very short timescales (**Figure 2.8**). The traces were fit to a single exponential to give $k_f = 7(3) \times 10^9$ s^{-1} for formation of Fe(II).

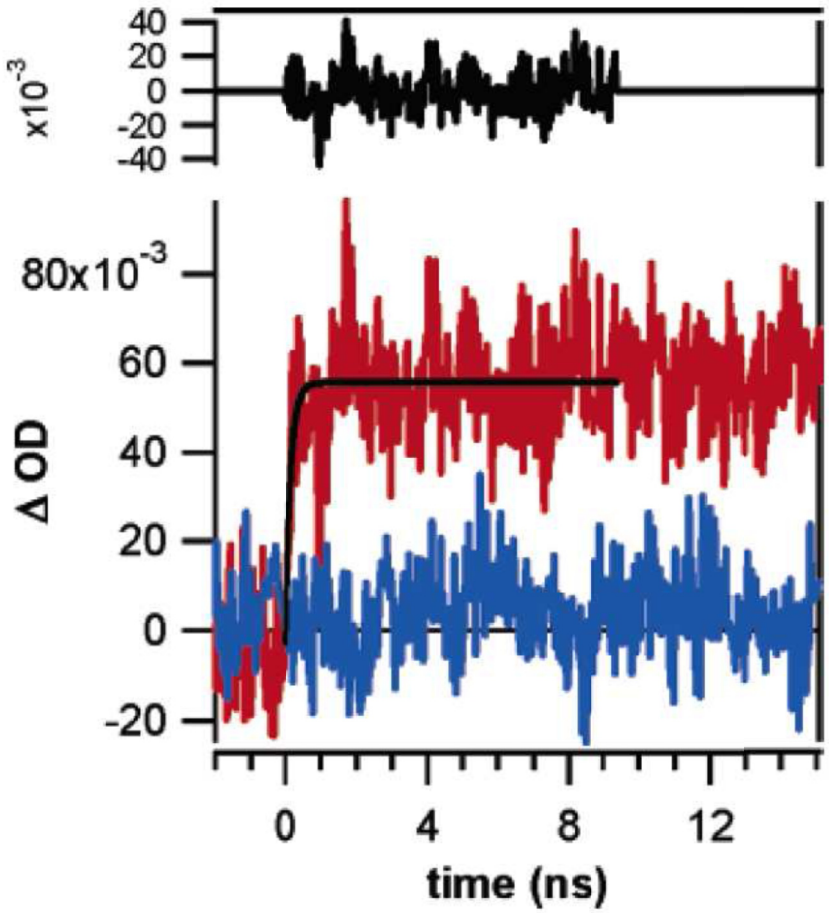

Figure 2.8. Transient absorbance at 442 nm of iNOSoxy alone (8 μM, blue) and in the presence of excess **5** (red) with λ_{ex} = 355 nm. The red trace shows the rapid formation of the ferrous heme, fit to one exponential (k_f = 7(3) x 10^9 s^{-1}, black) with the residual shown above.

Although the demonstration of very rapid electron transfer to a heme active site represents a step toward the goal of observing high-valent intermediates, our electron delivering wires block access to substrate channels. We have exploited this property of channel binders in the construction of highly selective amine oxidase inhibitors by manipulation of the linker elements of wire structures.[11]

A Novel Surface-Binding Wire

Nitric oxide synthase (NOS) is a heme monooxygenase that catalyzes the five-electron oxidation of L-arginine and O_2 to citrulline and nitric oxide (NO). NOS effects

this transformation in two turnovers, producing N^G-hydroxy-L-arginine (NHA) as an enzyme-bound intermediate, requiring three electrons from its reductase domain. Each turnover is expected to proceed through a mechanism similar to that of cytochrome P450 (although the two turnovers may utilize a different species for substrate oxidation), central to which are two slow electron transfer (ET) events.[12, 18-22] The first ET event reduces the resting, substrate-bound heme to the ferrous state, which then binds oxygen to create the last observable intermediate (ferric-superoxo).[20, 23] It is thought that the second ET event, where the electron is supplied by the cofactor tetrahydrobiopterin (BH_4), produces one or more high-valent heme species, with substrate oxidation possibly occurring from a ferryl-porphyrin$^{+\bullet}$ intermediate (Compound I).[20, 24] The sluggishness of the second ET step, however, has so far prevented the characterization of high-valent intermediates in the catalytic cycle in solution.[12, 20, 25] Cryoreduction of the heme domain of ferric-superoxo endothelial NOS at 77 K leads to the formation of a ferric-peroxo species.[12] Annealing at 165 K results in conversion to the product state without the appearance of intermediates. These data suggest that O-O bond cleavage is slower than reaction with substrate.

By employing laser-induced ET to reduce the active-site heme very rapidly, it should be possible to observe high-valent intermediates that follow in the catalytic cycle. Toward this end, we and others have developed photoactive electron tunneling wires to deliver electrons and holes to and from the deeply buried heme active sites in P450cam[8, 26-27] and NOS.[16, 28-30] Importantly, one of the NOS wires, tmRu-F_9bp (**Scheme 2.4**), can potentially probe the catalytic cycle, since it binds tightly and specifically to the oxidase domain of the inducible form of the enzyme (iNOSoxy) in a region that is *distant* from

the active site.[17] Here we demonstrate that an imidazole-ligated heme in tmRu-F_9bp:iNOSoxy can be photoreduced several million times faster (k_{ET} = 2(1) × 10^7 s^{-1}) than the physiological ET reaction.

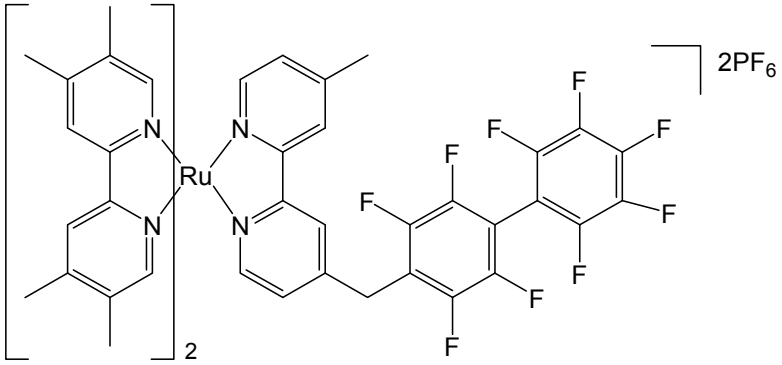

Scheme 2.4. tmRu-F_9bp.

2.3 Materials and Methods

General

The tmRu-F_9bp complex was synthesized as described previously.[8-9, 31] Tetramethylphenylenediamine (TMPD) was obtained from Aldrich and vacuum-sublimed before use. Tetrahydrobiopterin (BH_4, Aldrich) was stored under argon at -20 °C. All other chemicals were used as received from Sigma, JT Baker, Fischer, EM Sciences, and Mallinckrodt. UV-visible absorption spectra were acquired on an Agilent 8453 UV-visible spectrophotometer. Gel electrophoresis was run on a Phast System (Pharmacia) with 8–25 percent gradient precast agarose gels and SDS buffer strips. Samples were loaded in 4x SDS buffer and stained with Coomassie blue. Samples were run against Precision Plus All-Blue standards (BioRad).

iNOSoxy Expression and Purification

The heme domain of iNOS with a C-terminal His_6 tag was overexpressed in *E. coli* and purified as described previously [32] with several exceptions. Briefly, expression cells were subjected to two rounds of chemical lysis by pelleting and resuspension in 40 mL of B-PER lysis buffer (protein extraction reagent B, Pierce). The lysis buffer included a cocktail of protease inhibitors (10 μg/mL benzamidine, 5 μg/mL leupeptin, 1 μg/mL each pepstatin, antipain, and chymostatin, and ~ 500 μM Pefabloc (Roche)) as well as 100 μg/mL DNase, 100 μg/mL RNase, ~ 500 μg/mL lysozyme, and 20 mM imidazole per liter of cells. The suspension was centrifuged and the supernatant was loaded directly onto a His_6 immobilized metal-ion affinity chromatography column (5 mL Ni^{2+}:HisTrap, Amersham). Once the protein was completely loaded, it was washed with 20 column volumes of 20 mM imidazole in 50 mM NaP_i/300 mM NaCl/pH 8. The protein was eluted with 150 mM imidazole and concentrated to ~ 3 mL in an Amicon Ultra centrifugation device (10,000 MWCO, Millipore). The concentrated sample was then further purified over a size-exclusion column, as described previously.[32] The anion exchange column was omitted when ≥ 95 percent purity was confirmed by UV-visible spectroscopy and gel electrophoresis. The purified protein was concentrated to ~ 200 μM, divided into 100 μL aliquots, and stored in 50% glycerol at -80 °C.

Sample Preparation

Small aliquots of iNOSoxy were thawed and exchanged into phosphate buffer (50 mM KP_i, 50 mM KCl, pH 7.4) using a PD-10 desalting column (BioRad) immediately before use. The position of the heme Soret maximum (422 nm) confirmed the presence of low-spin, water-bound heme.[17, 32] The heme protein concentration was determined using

ε_{422} = 75 $mM^{-1}cm^{-1}$ per unit heme.[17] For the inhibitor-bound samples, imidazole (400-500 μM) was added, and binding was confirmed by a Soret shift to 428 nm.[17, 32] For substrate-bound, pterin-free samples, 1 mM arginine was added to dilute (~ 2–20 μM) iNOSoxy and allowed to incubate at 4 °C for approximately 30 min. In the absence of pterin (BH_4), only partial conversion to a high-spin heme (λ_{max} = 398 nm [32-33]) was observed. For substrate- and pterin-bound samples, fresh BH_4 solutions were prepared daily. Phosphate buffer was thoroughly deoxygenated by bubbling with argon for ≥ 10 min. Solid BH_4 was added to the degassed buffer under a counter-flow of argon. Dilute iNOSoxy (~ 2–20 μM) was deoxygenated by at least 30 evacuation-Ar backfill cycles, taking care to avoid bubbling of the solution. Aliquots of concentrated, deoxygenated pterin and arginine stocks were then added to the protein solution, giving final concentrations of 100 μM BH_4 and 1 mM arginine. The solution was incubated for 2 h at 4 °C; binding of BH_4 and arginine was confirmed by a Soret shift to 396 nm.[34-35]

For quenching experiments, 1 M ascorbate stock solutions were prepared daily by dissolving ascorbate in thoroughly deoxygenated 1 M KOH. Ascorbate (1 M) and solid TMPD were added to deoxygenated protein solutions under a counter-flow of argon.

Transient Spectroscopy

Luminescence decay and transient absorption measurements were made as described previously.[7, 36-37] The ~ 8 ns, 480 nm excitation pulses were produced by a Nd:YAG pumped optical parametric oscillator. Data were collected at 1×10^9 samples s^{-1} using a LeCroy digital oscilloscope. Transient absorbance data were converted from intensity to absorbance using the following expression (Eq. 2.3):

$$\Delta Abs = -\log\left(\frac{I}{I_0}\right) \qquad (2.3)$$

where I is the intensity of light transmitted through the sample excitation volume, and I_0 is the average transmitted light intensity during the 200 ns prior to the laser shot. Luminescence decay curves and transient absorbance traces were fit to one, two, or three exponentials using a nonlinear least-squares algorithm (Eq. 2.4, Igor Pro):

$$I(t) = c_0 + \sum_n c_n e^{-k_n t} \qquad (2.4)$$

Each experiment was repeated at least three times unless indicated otherwise.

Determination of $Ru^I \rightarrow Fe^{III}$ ET Rate Constants

At a given time after excitation, the absorbance observed at a given wavelength (λ) between 400 and 450 nm is (Eq. 2.5):

$$\Delta Abs = \left(\varepsilon_{Fe^{II}} - \varepsilon_{Fe^{III}}\right)\left[Fe^{II}\right] + \left(\varepsilon_{*Ru^{II}} - \varepsilon_{Ru^{II}}\right)\left[*Ru^{II}\right] + \left(\varepsilon_{Ru^{I}} - \varepsilon_{Ru^{II}}\right)\left[Ru^{I}\right] \qquad (2.5)$$

Since ascorbate, TMPD, and $TMPD^{+\bullet}$ do not absorb strongly in this region (under the conditions of these experiments, **Figure 2.9**), the contributions of these species were neglected. Owing to substantial populations of unbound Ru-complex, the absorbance changes at these wavelengths due to depopulation of Ru^{II} and formation of $*Ru^{II}$ are large compared to those for Fe^{II} formation because $[*Ru^{II}] >> [Fe^{II}]$. Moreover, the presence of both free and iNOSoxy-bound wire complicates the transient absorbance kinetics. In fitting these data, we were unable to identify a phase that was distinct from those corresponding to $*Ru^{II}$ decay in bound and free wires, and that reliably could be attributed to intraprotein ET from Ru^{I} to Fe^{III} (k_{ET}).

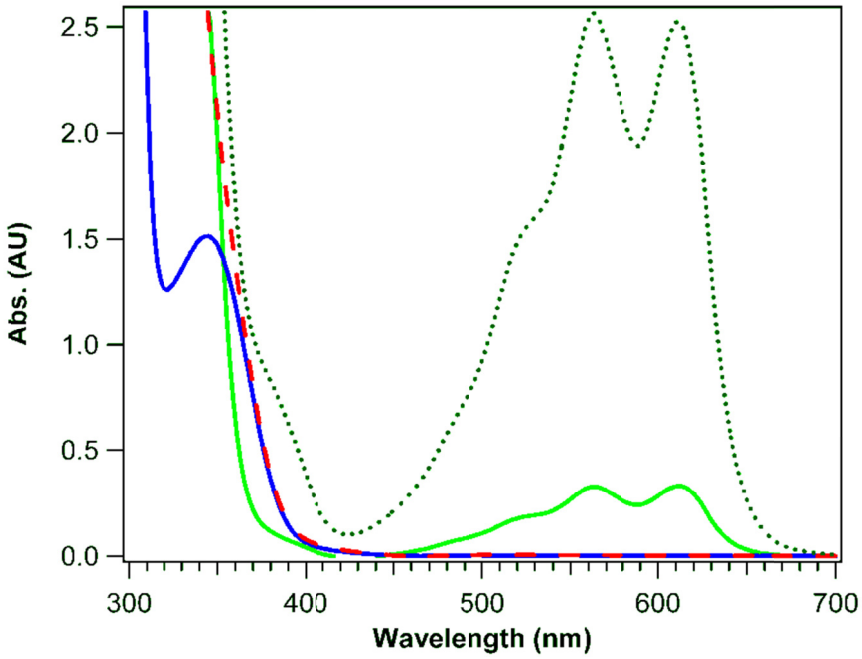

Figure 2.9. UV/visible absorption spectra of ascorbate and TMPD. Spectra were taken in the presence of tmRu-F_9bp (14 μM) before (blue and light green traces) and after (red dashed and green dotted traces) photolysis at 480 nm and then corrected for absorbance due to tmRu-F_9bp. For the TMPD radical cation, ε_{565} = 12.5 mM^{-1} cm^{-1} and ε_{612} = 12.0 mM^{-1} cm^{-1}.

In order to characterize the Ru^{I} to Fe^{III} ET kinetics, we developed a procedure to remove the $*Ru^{II}$ contribution from the transient absorbance kinetics. The isosbestic point for low-spin, imidazole-bound Fe^{III} iNOSoxy and the product Fe^{II} species occurs at 438 nm. In each experiment, therefore, transient absorbance of the Im-iNOSoxy/wire/quencher system at 438 nm reflects the $*Ru^{II}$ bleach and recovery, but contains no contribution from iNOSoxy. Using an experimentally validated $*Ru^{II}$-Ru^{II} difference spectrum, we determined scaling factors by which we could multiply the 438 nm transient signals to produce estimates of the $*Ru^{II}$ contributions to the observed kinetics at several other wavelengths ([$*Ru^{II}$-Ru^{II}]: $\Delta\varepsilon_{452}/\ \Delta\varepsilon_{438}$ = 1.12, $\Delta\varepsilon_{425}/\ \Delta\varepsilon_{438}$ = 0.66). The calculated $*Ru^{II}$ signals were subtracted from the observed transient kinetics to produce signals corresponding to the time dependence of [Fe^{II}]. Transient Ru^{I} absorbance

was neglected because its Δε values are < 10 percent of those for [Fe^{II}-Fe^{III}] (**Figure 2.10**). The resulting corrected traces were then fit to single exponential functions according to Eq. 2.4.

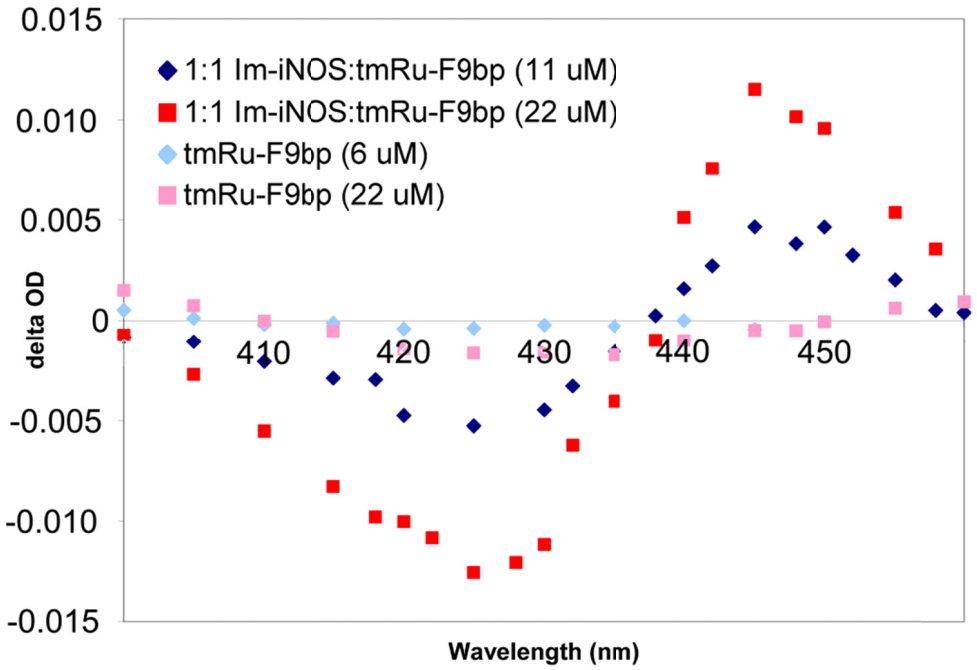

Figure 2.10. Transient absorbance at 2 μs of quenched tmRu-F_9bp in the presence and absence of one equivalent of Im-iNOSoxy, demonstrating the negligible contribution of Ru(I) absorbance to the overall kinetics. Samples contain 10 mM ascorbate and saturated tmpd. λ_{ex} = 480 nm.

2.4 Results and Discussion

Binding of tmRu-F_9bp to iNOSoxy

We have previously shown that tmRu-F_9bp (Chart 1) binds to iNOSoxy independently of substrate and BH_4 with a dissociation constant of ~ 1 μM.[17] Remarkably, this wire binds at a site distant from the active-site channel, as demonstrated by the finding that a known channel-binding wire does not displace tmRu-F_9bp from the enzyme.[17] While the precise binding site has not been definitively established, Förster

energy transfer measurements indicate that it may be in the hydrophobic pocket thought to be the docking site for the iNOS reductase domain.[17, 38] Experiments with $Ru(bpy)_3^{2+}$ show that the photosensitizer alone does not bind to the enzyme (**Figure 2.11**), suggesting that the perfluorobiphenyl unit is largely responsible for the strong association of the wire with a hydrophobic iNOSoxy surface region.

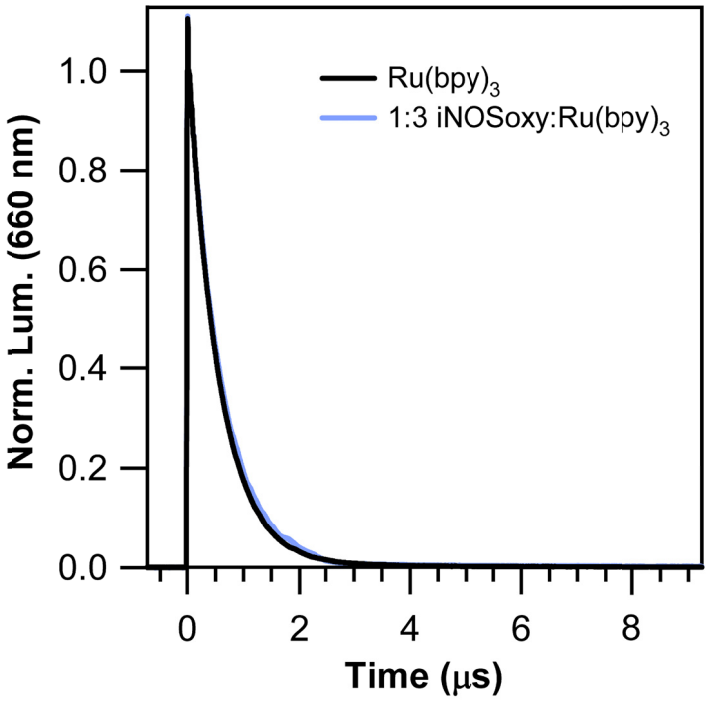

Figure 2.11. Transient luminescence of $Ru(bpy)_3^{2+}$ in the presence and absence of iNOSoxy. These data demonstrate that $Ru(bpy)_3^{2+}$ itself does not bind to iNOSoxy, even when present in threefold excess. λ_{ex} = 480 nm.

Quenching of the Bound Ru-Wire

In previous work, we described Ru-diimine wires that reduce the heme of cytochrome P450 directly upon photoexcitation.[8] In these experiments the wire termini ligated the iron center, providing an efficient through-bond coupling pathway between the sensitizer and the heme. In contrast, the Ru-wire described here does not directly photoreduce the heme, so we employed a flash/quench method with exogenous

reductants to produce Fe^{II}.[6] In this experiment, a quencher (Q) reduces the photoexcited sensitizer to create a strongly reducing species (Ru^{I} in **Scheme 2.5**). In the absence of other electron acceptors, the lifetime of Ru^{I} is dependent on the rate of recombination with the oxidized quencher (k_r in **Scheme 2.5**). Because Q^+ and Ru^{I} are present at low and equal concentrations, recombination is slow (ms timescale) and heme reduction competes effectively.

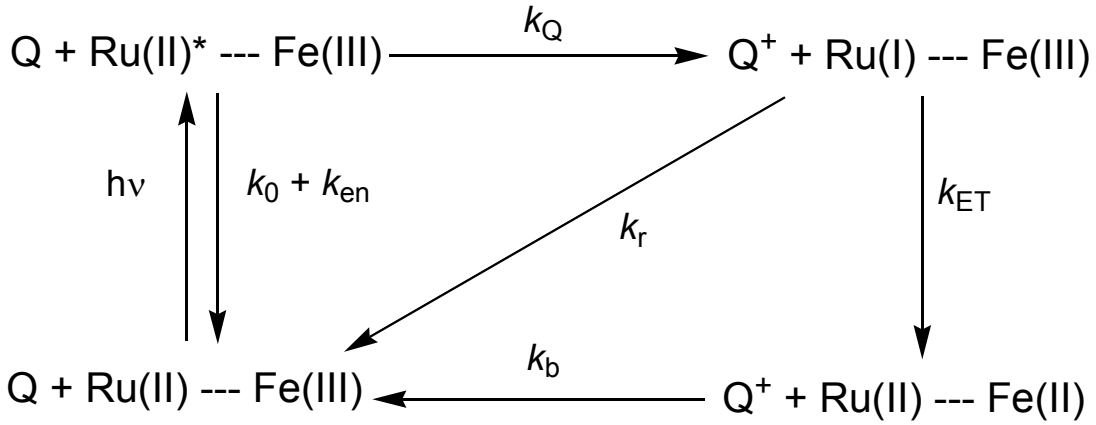

Scheme 2.5. Representation of the reversible flash/quench experiment employed in this work. For simplicity, TMPD and ascorbate are represented together as Q. In a successful flash/quench experiment, quenching must compete with intrinsic relaxation (k_0) and energy transfer (k_{en}) for depletion of the Ru^{II} excited state ($k_Q[Q] \geq k_0 + k_{en}$); and electron transfer (k_{ET}) must be faster than recombination between oxidized quencher and reduced sensitizer ($t_{½} = 1/k_r[Ru^{I}]_0$).

Owing to its high solubility in water and lack of spectral interference with heme Soret changes, ascorbate (Asc) is an attractive choice as a quencher for this system. Even at high concentrations (10 mM), however, Asc quenching produces only small yields of Fe^{II} (**Figures 2.12 and 2.13**). TMPD (**Scheme 2.6**) is a better quencher than Asc, but has limited solubility in water.[39-40] Further, TMPD autoxidizes to create a soluble bright blue cation radical in aqueous media.[41] Under conditions necessary for efficient excited-state quenching, the production of the radical rapidly turns the solution dark blue, obscuring small transient changes in the heme spectrum.

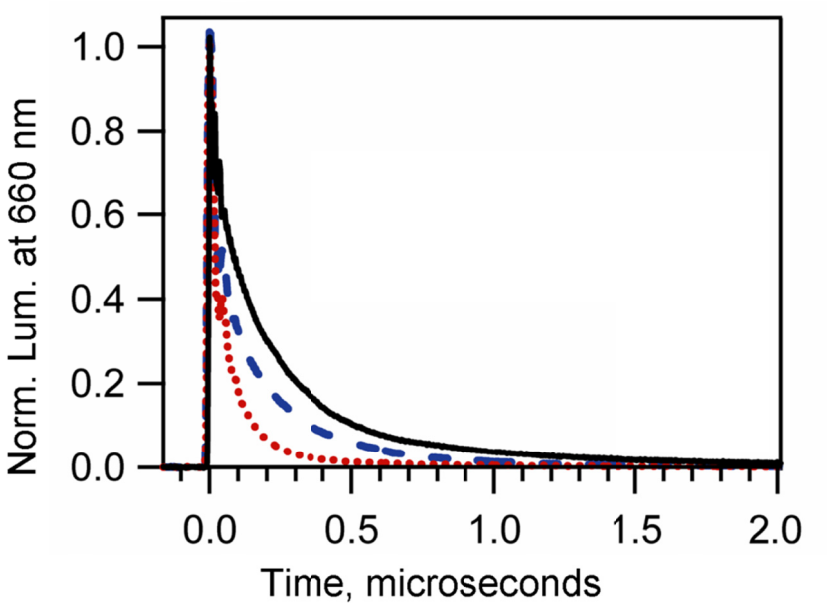

Figure 2.12. Luminescence decay of 6.2 μM tmRu-F_9bp bound to equimolar Im-iNOSoxy in the absence of quenchers (black line) and in the presence of 10 mM Asc (blue dashes) or 10 mM Asc and saturated TMPD (red dots). λ_{ex} = 480 nm and λ_{obs} = 660 nm.

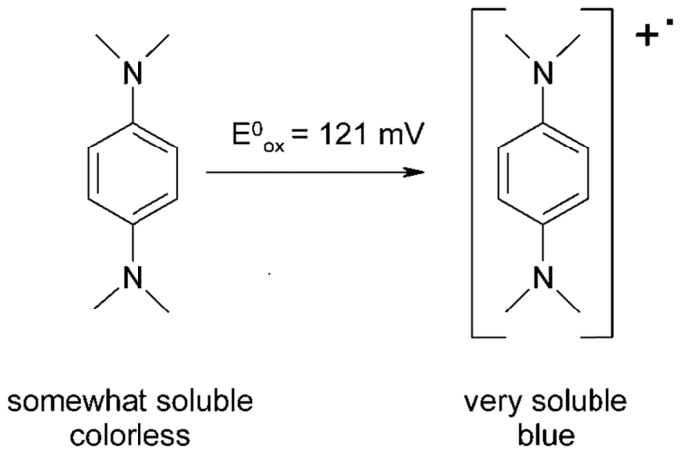

Scheme 2.6. TMPD, a water-soluble reductive quencher, in its reduced and oxidized forms.

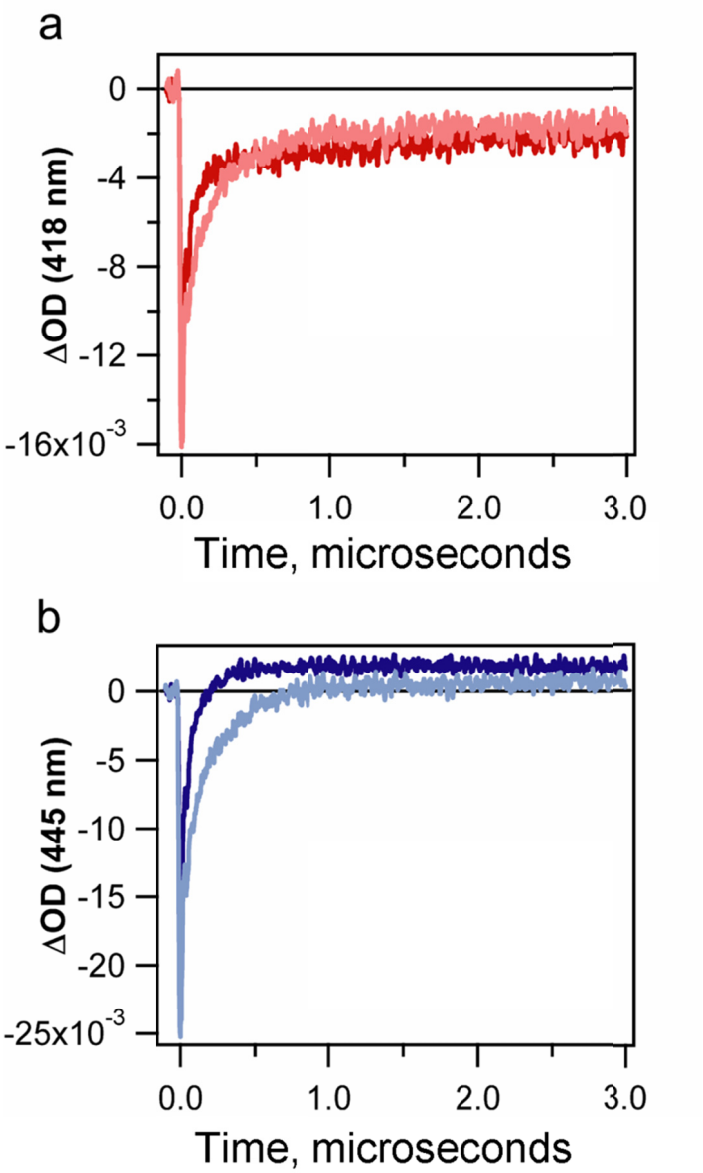

Figure 2.13. Transient absorbance of 1:1 mixtures of tmRu-F_9bp and Im-iNOSoxy (6.2 μM) in the presence of 10 mM Asc with (darker traces) and without (lighter traces) saturated TMPD. λ_{ex} = 480 nm. a) λ_{obs} = 418 nm. b) λ_{obs} = 445 nm. The addition of TMPD increases the yield of reduced heme.

These problems were overcome by employing both quenchers.[42-43] In a sample containing 10 mM Asc with saturated TMPD, the superior quenching capability of TMPD can be exploited (**Figure 2.10**, red dotted trace) while Asc serves to keep the

TMPD reduced. With Asc present, $TMPD^{+\bullet}$ does not accumulate, even after 60 min. of photoexcitation in the presence of tmRu-F_9bp.

Rapid Production of Reduced iNOSoxy

Single wavelength transient absorbance measurements with imidazole-bound iNOSoxy in the presence of one equivalent of tmRu-F_9bp, 10 mM Asc, and saturated TMPD reveal that photochemically generated Ru^I disappears with concomitant formation of a new Fe species within 50 ns of excitation at 480 nm (**Figure 2.14**).

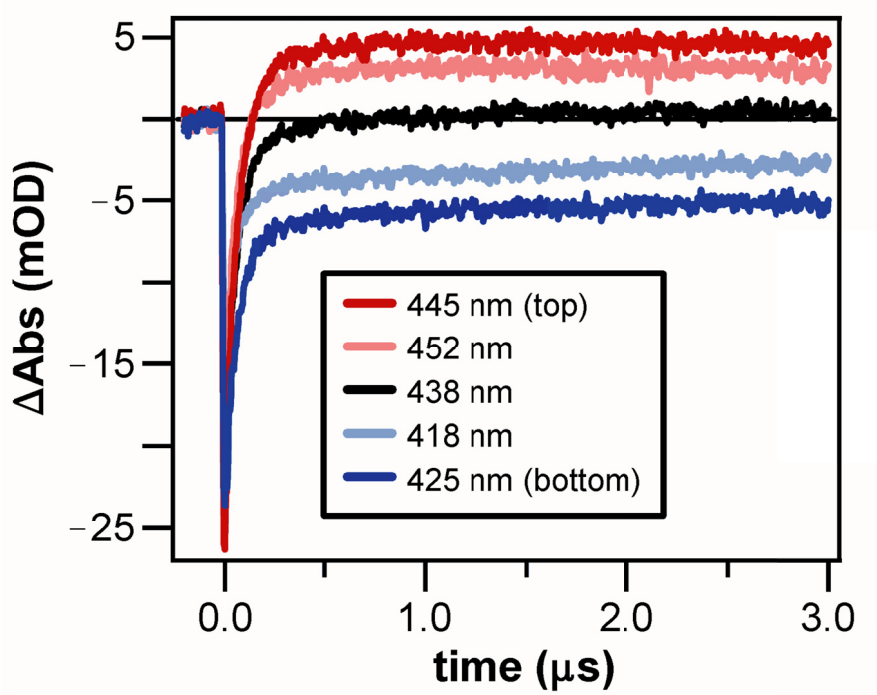

Figure 2.14. Transient absorbance of quenched Im-iNOSoxy bound to 1 equivalent of tmRu-F_9bp (11 μM with 10 mM Asc and saturated TMPD). λ_{ex} = 480 nm.

A difference spectrum constructed from the single-wavelength data at 2 μs (**Figure 2.15**) shows the bleach of the Im-Fe^{III} Soret absorption at 428 nm and increased absorbance to the red with a difference-spectrum maximum at 445 nm. The rate of decay of Ru^I and reappearance of Ru^{II} is approximately equal to the rate of changes in the Soret region. Given that Ru^{II} is reformed, the most likely explanation for spectral changes

between 400 and 450 nm is Ru^{I} to Fe^{III} ET, which produces a new Fe^{II} heme species. Control experiments with $Ru(bpy)_3^{2+}$ indicate that the tmRu-F_9bp perfluorobiphenyl moiety is required for heme reduction (**Figure 2.16**). In the presence of $Ru(bpy)_3^{2+}$ and quenchers, transient absorbance traces show only the production of Ru^{I}.

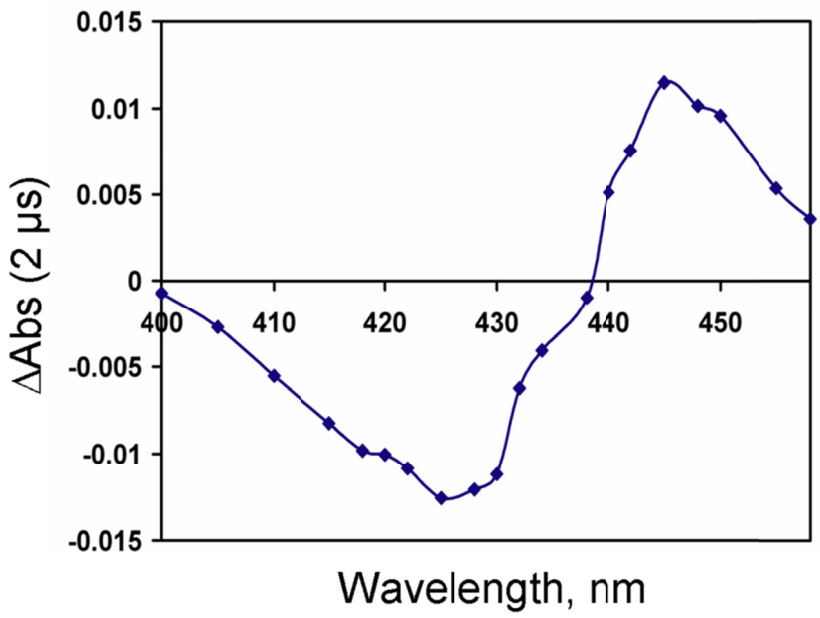

Figure 2.15. Transient absorbance of a 1:1 mixture of Im-iNOSoxy and tmRu-F_9bp (22 μM with 10 mM Asc and saturated TMPD) showing a characteristic Fe(III/II) difference spectrum. Individual points were taken from single wavelength transient absorbance traces at 2 μs after excitation at 480 nm.

In order to estimate the specific rate of Fe^{II} formation, $*Ru^{II}$ contributions were subtracted from the transient absorbance data as described in Materials and Methods (representative single-wavelength traces are shown in **Figure 2.17**). The traces (a minimum of four wavelengths from each of four different experiments completed on different days) were fit to a single exponential function: $k_{ET} = 2(1)\times10^7\ s^{-1}$.

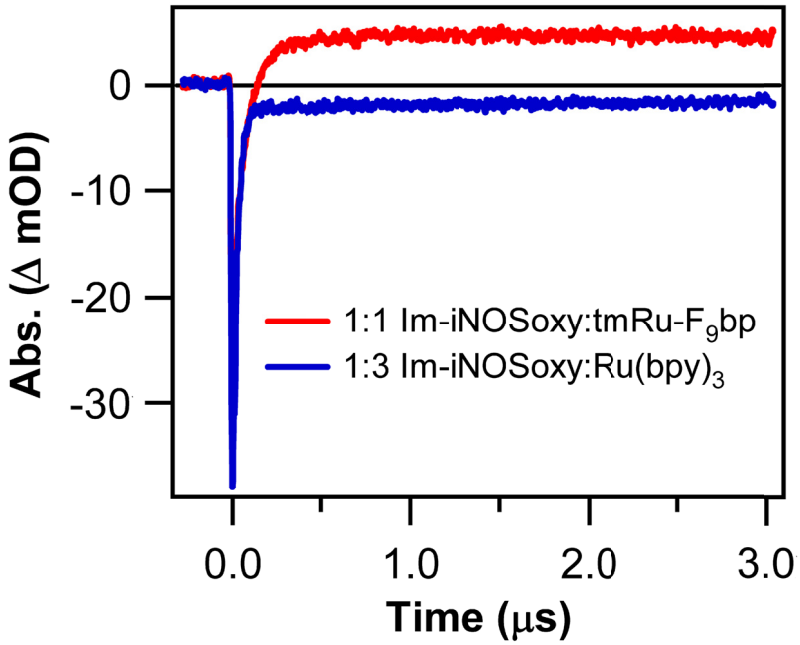

Figure 2.16. Transient absorbance of imidazole-bound iNOSoxy in the presence of tmRu-F_9bp or $Ru(bpy)_3^{2+}$ and quenchers (10 mM ascorbate + saturated TMPD). λ_{ex} = 480 nm, λ_{obs} = 445 nm. In the absence of the perfluorobiphenyl wire, quenched $Ru(bpy)_3^{2+}$ does not produce Fe^{II}. The long-lived bleach is due to Ru^{I}.

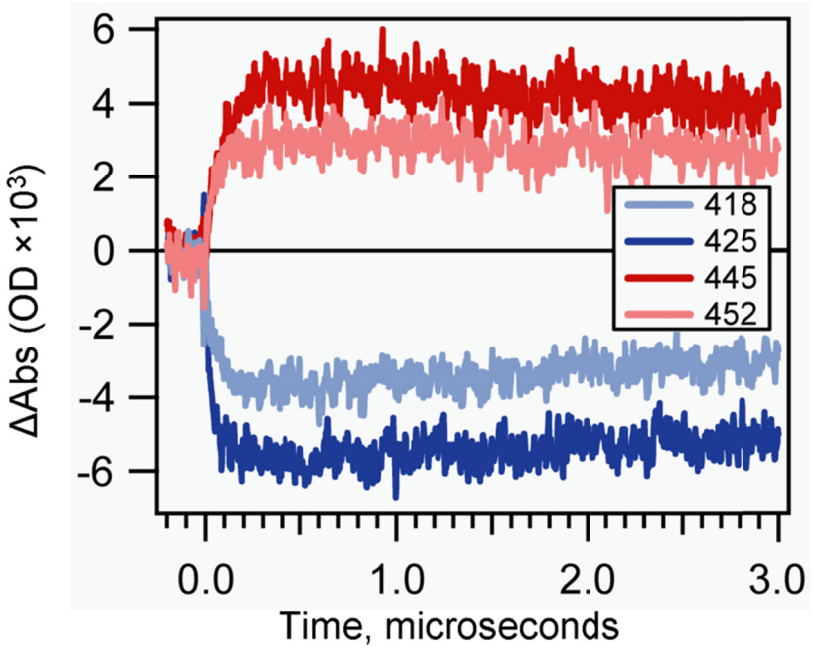

Figure 2.17. Transient absorbance of Im-iNOSoxy bound to 1 equivalent of tmRu-F_9bp (11 μM with 10 mM Asc and saturated TMPD) corrected for absorbance due to $*Ru^{II}$: k_{ET} = $2(1)\times10^7$ s^{-1}; λ_{ex} = 480 nm.

This is a remarkably rapid reduction given the estimated Ru-heme distance of 20.2 Å[17] and the absence of a through-bond pathway to the heme. Given its slim profile, hydrophobicity, and potential to π-stack with aromatic residues, the perfluorobiphenyl moiety of tmRu-F_9bp may intercalate into the protein interior, leaving open the possibility of a through-wire hopping mechanism.[28]

Identity of the Reduced Species

In order to determine the nature of the product of electron transfer to the heme, the six-coordinate Fe^{III}-Im species was reduced under equilibrium conditions for comparison with the transient data. Reaction of Fe^{III}-Im with sodium dithionite in a glove box under an inert atmosphere, followed by removal of excess dithionite on a size-exclusion (PD-10) column equilibrated with 10 mM imidazole, produced a species with the absorption spectrum shown in **Figure 2.18**.

Reduction of NOS has been extensively studied.[25, 35, 44-47] Six-coordinate ferrous-NO and -CO species have been characterized by several investigators;[35, 46-47] and, in the absence of arginine and BH_4, it has been shown that these six-coordinate species are unstable. Addition of CO (or NO) to five-coordinate Fe^{II} causes a red-shift in the Soret band to 444 nm (or 440 nm).[35] The 444 nm band blue-shifts over time to 421 nm, which suggests that a species analogous to the inactive P420 form of cytochrome P450 is produced. It has been proposed that the axial thiolate is not bound to the heme iron in the 421 nm species[35, 47] of that the thiolate is protonated.[48]

The blue-shift of the iNOSoxy Soret peak upon dithionite reduction (**Figure 2.18**, inset) demonstrates that the red-shifted transient Fe^{II} species produced by photochemical heme reduction likely has different axial coordination. The steady-state Fe^{II} absorption

spectrum is in good agreement with that reported for *Drosphila melanogaster* DHR51, a heme protein believed to possess axial Cys and His ligands.[49] Similar spectra have been reported for Fe^{II} forms of mutant cytochrome *c* and myoglobin engineered to have axial Cys and His ligands.[50-51] In each of these Fe^{II} proteins, the Soret maximum is slightly blue-shifted relative to its position in the Fe^{III} form, indicating the presence of a low-spin Fe^{II} heme in which imidazole remains bound but the thiolate ligand has been displaced. Further, five-coordinate ferrous iNOSoxy has been generated, showing a blue-shift of the Soret from the ferric species similar to the spectrum in **Figure 2.18**.[35]

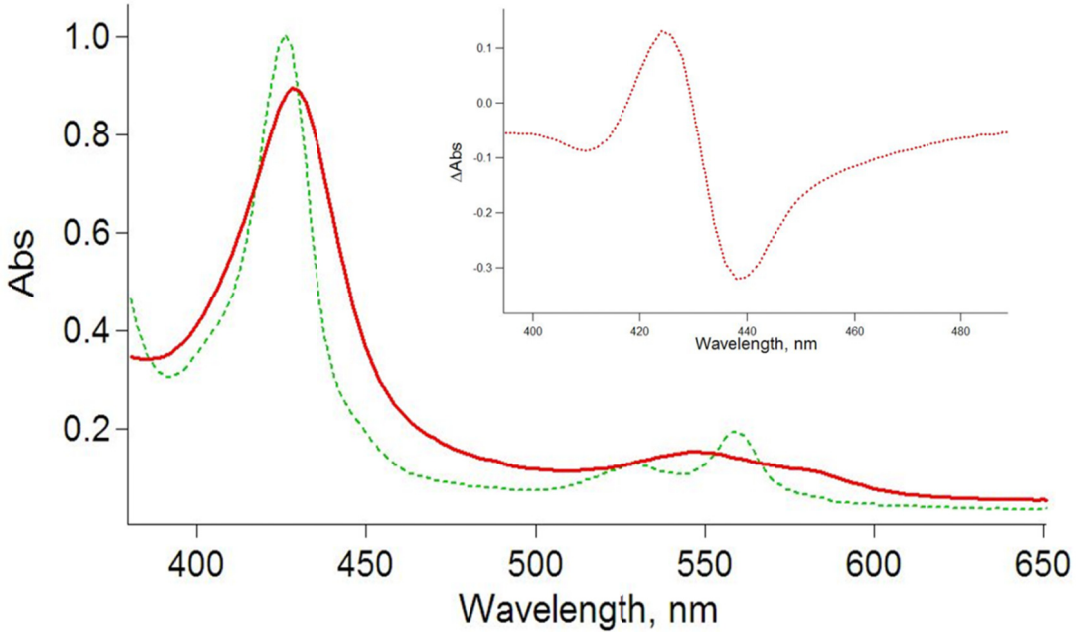

Figure 2.18. Steady-state spectra of ferric-imidazole (red solid line) and the reduced species (green dashed line). Inset: The difference spectrum generated upon reduction (red dotted line).

In contrast, the red-shifted Soret band found for photochemically reduced iNOS is analogous to that resulting from cryoreduction of ferric cytochrome P450. Irradiation of six-coordinate low-spin Fe^{III} P450 in a frozen matrix produces a low-spin, presumably six-coordinate Fe^{II} product.[13] Annealing at higher temperatures leads to the high-spin Fe^{II}

product that is observed under equilibrium conditions. We suggest that the transient Fe^{II} iNOS species formed by photochemical reduction contains a low-spin Fe^{II} heme with axial Cys and imidazole ligands. In our experiment, this species is likely reoxidized by $TMPD^{+\bullet}$ before loss of axial ligation, which would generate the species observed under equilibrium conditions.

2.5 Concluding Remarks and Discussion

We have developed a system in which the heme of inducible nitric oxide synthase can be photoreduced rapidly without interfering with substrate/cofactor binding. Employing flash/quench experiments with a surface-binding Ru-diimine wire in combination with reductive quenchers, we observed ET to the imidazole-bound heme of iNOSoxy fully seven orders of magnitude faster than the natural reduction. This finding represents an important step toward our goal of identifying reactive intermediates in the catalytic cycles of heme monooxygenases.

Interestingly, however, the product of this ET reaction is a six-coordinate heme. In contrast, the product of steady-state reduction of the heme is consistant with either a five-coordinate species with imidazole ligation or a complex where the negative axial thiolate ligand becomes protonated forming a neutral thiol ligand. On the millisecond timescale this six-coordinate species is stable, however, over the long term it will decay to the more thermodynamically favored five-coordinate or neutral thiol complex. This decay highlights the inherent instability of the thiolate-ligated heme complex.

Upon closer inspection of the environment around the thiolate ligand, one finds a collection of three hydrogen bond (H-bond) donors all directed toward the thiolate.

Comparison of iNOSoxy with other NOS enzymes reveals that these three hydrogen bond donors are universally conserved, with not a single exception. This high level of conservation underscores their potential importance. Not only are they conserved in nitric oxide synthases, but the crystal structures of other heme thiolate enzymes reveal similarly conserved hydrogen bond donors in all. Cytochrome P450s (cyt. P450) all contain three H-bond donors; chloroperoxidase (CPO) contains only two such donors.

When analyzing these polypeptide chains, one finds that in cyt. P450 and CPO all three donors in the proximal heme environment come not from amino acid side-chains but from amide protons in the backbone of the polypeptide chain. In NOS alone one and only one of the H-bond donors comes not from an amide but from the N-H of a tryptophan's indole ring, **Figure 2.19**. The universality of these H-bond donors pointing right at the axial thiolate ligand provokes questions of their function in the reactivity or stability or electronic tuning of these enzymes.

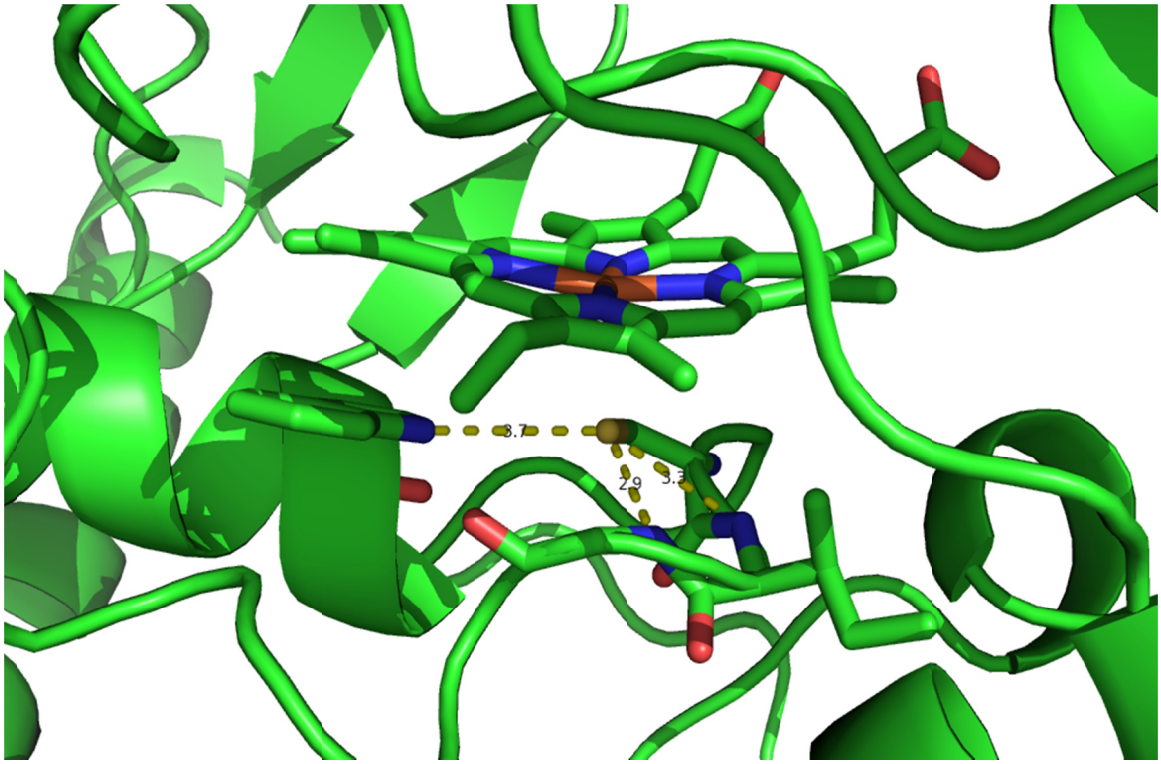

Figure 2.19. Close-up view of the heme center in a nitric oxide synthase showing the three hydrogen bond donors. The middle and the right are from amide groups on the protein backbone (2.9 and 3.3 Å) while the long H-bond on the left comes from a tryptophan (very long at 3.7 Å) (PDB file 2FLQ).

Others have attempted to investigate the possible roles of these H-bond donors in cyt. P450.[52-54] The replacement of a glutamine that provides one amide group with a proline forces a kink in the loop below the heme and obviously replaces the N-H bond in the glutamine backbone with a N-C bond, incapable of participating in H-bonding. This also removes a hydrogen bond from the side chain of the Gln to the carbonyl moiety of the cysteine residue. The combination of these two effects as well as the shift in the backbone resulting from introduction of a proline makes results difficult to deconvolude. The work suggests, however, that this H-bond donor (not even a legitimate hydrogen bond) shifts the reduction potential of the heme by about +40 mV (removing it makes the potential more negative by about 40 mV). Resonance Raman suggests that this H-bond

donor decreases the σ-donating ability of the thiolate significantly; its removal strengthens the iron-sulfur bond. They "conclude that the functions of the proximal hydrogen bonding network in $P450_{cam}$ are to stabilize the heme-thiolate coordination, and to regulate the redox potential of the heme iron."[54] While these conclusions seem reasonable, it is difficult to say the effect of a particular H-bond when several things are affected at once.

We wish to determine the role of these H-bond donors and support or refute the previous findings, but particularly to study their effects in NOS. This family of enzymes provides a unique opportunity, given that one of the H-bond donors comes not from the backbone but from a side chain, allowing for facile and systematic variation using site-directed mutagenesis. Several such mutations have previously been made in NOS and characterized by resonance Raman.[55-56] No further characterization has been reported.

One other mutant of interest replaced the tryptophan with a histidine, preserving and possibly increasing the H-bond donor ability of the group. In this mutant, researchers actually saw a slower kinetics profile and possibly a new intermediate by stopped-flow spectroscopy.[25] No further characterization was done and the new intermediate, based solely upon the position of the Soret band, was suggested to be Compound I (**Scheme 2.3**, the ferryl complex in blue). The lifetime of this new intermediate is on the order of a couple of seconds before decaying to product. Compound I is formally a Fe(V) complex, with a ferryl and another radical cation sometimes found on the porphyrin ring. The likelihood of such a species living for that length of time is incredibly low as it will be very reactive, making its assignment as Compound I doubtful.[14] No other investigations into the role of this H-bond donor have been made.

We propose to investigate the role of these H-bond donors by systematically varying the functional groups on this side chain in question through the use of site-directed mutagenesis. The native tryptophan will be replaced with histidine, phenylalanine, or tyrosine. Histidine can also participate in hydrogen bonding, but lacks the ability to π-stack with the porphyrin ring. Phenylalanine complements the histidine mutation in that it can π-stack but cannot hydrogen bond. The tyrosine can also π-stack, but the electronics should be significantly altered due to the presence of the hydroxyl group on the aryl ring, which is at an angle that should prohibit hydrogen bonding with the thiolate. These three mutants will be expressed and thoroughly characterized using the tools of modern bioinorganic chemistry to investigate the thermodynamics of the resulting active site and its reactivity (EPR, electrochemistry, single turnover experiments, etc.). These studies should provide valuable insight into the specific role of these hydrogen bond donors and their purpose in NOS and other heme thiolate enzymes, and this work will be the focus of the bulk of this thesis.

2.6 References

1. Finkel, T., and Holbrook, N. J. (2000) Oxidants, oxidative stress and the biology of ageing, *Nature 408*, 239.
2. Arnon, D. I. (1959) Conversion of light into chemical energy in photosynthesis, *Nature 184*, 10.
3. Marcus, R. A., and Sutin, N. (1985) Electron transfers in chemistry and biology, *Biochimica Et Biophysica Acta 811*, 265.
4. Gray, H. B., and Winkler, J. R. (1996) Electron transfer in proteins, *Annu. Rev. Biochem. 65*, 537.
5. Marcus, R. A. (1956) On the theory of oxidation-reduction reactions involving electron transfer .1, *J. Chem. Phys. 24*, 966.
6. Chang, I.-J., Gray, H. B., and Winkler, J. R. (1991) High-driving-force electron transfer in metalloproteins: Intramolecular oxidation of ferrocytochrome *c* by ru(2,2'-bipyridine)$_2$(imidazole)(histidine-33)$^{3+}$, *J. Am. Chem. Soc. 113*, 7056.
7. Low, D. W., Winkler, J. R., and Gray, H. B. (1996) Photoinduced oxidation of microperoxidase-8 - generation of ferryl and cation-radical porphyrins, *J. Am. Chem. Soc. 118*, 117.
8. Dunn, A. R., Dmochowski, I. J., Winkler, J. R., and Gray, H. B. (2003) Nanosecond photoreduction of cytochrome p450cam by channel-specific ru-diimine electron tunneling wires, *J. Am. Chem. Soc. 125*, 12450.
9. Dunn, A. R. (2003) Sensitizer-linked substrates as probes of heme enzyme structure and catalysis, In *Chemistry*, p 216, California Institute of Technology, Pasadena.
10. Hartings, M. R., Kurnikov, I. V., Dunn, A. R., Winkler, J. R., Gray, H. B., and Ratner, M. A. (2010) Electron tunneling through sensitizer wires bound to proteins, *Coord. Chem. Rev. 254*, 248.
11. Contakes, S. M., Nguyen, Y. H. L., Gray, H. B., Glazer, E. C., Hays, A. M., and Goodin, D. B. (2007) Conjugates of heme-thiolate enzymes with photoactive metal-diimine wires, In *Photofunctional transition metals complexes*, pp 177, Springer-Verlag Berlin, Berlin.
12. Davydov, R., Ledbetter-Rogers, A., Martásek, P., Larukhin, M., Sono, M., Dawson, J. H., Masters, B. S. S., and Hoffman, B. M. (2002) Epr and endor characterization of intermediates in the cryoreduced oxy-nitric oxide synthase heme domain with bound l-arginine or n^{g}-hydroxyarginine, *Biochemistry 41*, 10375.
13. Denisov, I. G., Makris, T. M., and Sligar, S. G. (2002) Cryoradiolysis for the study of p450 reaction intermediates, *Methods in Enzymology 357*, 103.
14. Rittle, J., and Green, M. T. (2010) Cytochrome p450 compound i: Capture, characterization, and c-h bond activation kinetics, *Science 330*, 933.
15. Berglund, J., Pascher, T., Winkler, J. R., and Gray, H. B. (1997) Photoinduced oxidation of horseradish peroxidase, *J. Am. Chem. Soc. 119*, 2464.
16. Whited, C. A., Belliston-Bittner, W., Dunn, A. R., Winkler, J. R., and Gray, H. B. (2008) Probing the heme-thiolate oxygenase domain of inducible nitric oxide synthase with ru(ii) and re(i) electron tunneling wires, *Journal of Porphyrins and Phthalocyanines 12*, 971.

17. Dunn, A. R., Belliston-Bittner, W., Winkler, J. R., Getzoff, E. D., Stuehr, D. J., and Gray, H. B. (2005) Luminescent ruthenium(ii)- and rhenium(i)- diimine wires bind nitric oxide synthase, *J. Am. Chem. Soc. 127*, 5169.
18. Griffith, O. W., and Stuehr, D. J. (1995) Nitric oxide synthases: Properties and catalytic mechanism, *Annu. Rev. Physiol. 57*, 707.
19. Groves, J. T., and Wang, C. C.-Y. (2000) Nitric oxide synthase: Models and mechanisms, *Curr. Opin. Chem. Biol. 4*, 687.
20. Zhu, Y., and Silverman, R. B. (2008) Revisiting heme mechanisms. A perspective on the mechanisms of nitric oxide synthase (nos), heme oxygenase (ho), and cytochrome p450s (cyp450s), *Biochemistry 47*, 2231.
21. Hurshman, A. R., Krebs, C., Edmondson, D. E., Huynh, B. H., and Marletta, M. A. (1999) Formation of a pterin radical in the reaction of the heme domain of inducible nitric oxide synthase with oxygen&#x2020, *Biochemistry 38*, 15689.
22. Wei, C.-C., Wang, Z.-Q., Tejero, J., Yang, Y.-P., Hemann, C., Hille, R., and Stuehr, D. J. (2008) Catalytic reduction of a tetrahydrobiopterin radical within nitric-oxide synthase, *J. Biol. Chem. 283*, 11734.
23. Robinet, J. J., Cho, K.-B., and Gauld, J. W. (2008) A density functional theory investigation on the mechanism of the second half-reaction of nitric oxide synthase, *J. Am. Chem. Soc. 130*, 3328.
24. Stuehr, D. J., Santolini, J., Wang, Z.-Q., Wei, C.-C., and Adak, S. (2004) Update on mechanism and catalytic regulation in the no synthases, *J. Biol. Chem. 279*, 36167.
25. Tejero, J., Biswas, A., Wang, Z.-Q., Page, R. C., Haque, M. M., Hemann, C., Zweier, J. L., Misra, S., and Stuehr, D. J. (2008) Stabilization and characterization of a heme-oxy reaction intermediate in inducible nitric-oxide synthase, *J. Biol. Chem. 283*, 33498.
26. Wilker, J. J., Dmochowski, I. J., Dawson, J. H., Winkler, J. R., and Gray, H. B. (1999) Substrates for rapid delivery of electrons and holes to buried active sites in proteins, *Angew. Chem. Int. Edit. 38*, 89.
27. Dmochowski, I. J., Dunn, A. R., Wilker, J. J., Crane, B. R., Green, M. T., Dawson, J. H., Sligar, S. G., Winkler, J. R., and Gray, H. B. (2002) Sensitizer-linked substrates and ligands: Ruthenium probes of cytochrome p450 structure and mechanism, *Method. Enzymol. 357*, 120.
28. Belliston-Bittner, W., Dunn, A. R., Nguyen, Y. H. L., Stuehr, D. J., Winkler, J. R., and Gray, H. B. (2005) Picosecond photoreduction of inducible nitric oxide synthase by rhenium(i)-diimine wires, *J. Am. Chem. Soc. 127*, 15907.
29. Nguyen, Y. H. L., Winkler, J. R., and Gray, H. B. (2007) Probing heme coordination states of inducible nitric oxide synthase with a re(i)(imidazole-alkyl-nitroarginine) sensitizer-wire, *J. Phys. Chem. B 111*, 6628.
30. Beaumont, E., Lambry, J. C., Gautier, C., Robin, A. C., Gmouh, S., Berka, V., Tsai, A. L., Blanchard-Desce, M., and Slama-Schwok, A. (2007) Synchronous photoinitiation of endothelial no synthase activity by a nanotrigger targeted at its nadph site, *J. Am. Chem. Soc. 129*, 2178.
31. Dmochowski, I. J. (2000) Probing cytochrome p450 with sensitizer-linked substrates, In *Chemistry*, p 305, California Institute of Technology, Pasadena.

32. Hurshman, A. R., and Marletta, M. A. (2002) Reactions catalyzed by the heme domain of inducible nitric oxide synthase: Evidence for the involvement of tetrahydrobiopterin in electron transfer, *Biochemistry 41*, 3439.
33. Wang, J. L., Rousseau, D. L., Abusoud, H. M., and Stuehr, D. J. (1994) Heme coordination of no in no synthase, *P. Natl. Acad. Sci. USA 91*, 10512.
34. Hurshman, A. R., and Marletta, M. A. (1995) Spectral characterization and effect on catalytic activity of nitric oxide complexes of inducible nitric oxide synthase, *Biochemistry 34*, 5627.
35. Abu-Soud, H. M., Wu, C., Ghosh, D. K., and Stuehr, D. J. (1998) Stopped-flow analysis of co and no binding to inducible nitric oxide synthase&#x2020, *Biochemistry 37*, 3777.
36. Kuciauskas, D., Freund, M. S., Gray, H. B., Winkler, J. R., and Lewis, N. S. (2001) Electron transfer dynamics in nanocrystalline titanium dioxide solar cells sensitized with ruthenium or osmium polypyridyl complexes, *J. Phys. Chem. B 105*, 392.
37. Dmochowski, I. J., Winkler, J. R., and Gray, H. B. (2000) Enantiomeric discrimination of ru-substrates by cytochrome $p450_{cam}$, *J. Inorg. Biochem. 81*, 221.
38. Garcin, E. D., Bruns, C. M., Lloyd, S. J., Hosfield, D. J., Tiso, M., Gachhui, R., Stuehr, D. J., Tainer, J. A., and Getzoff, E. D. (2004) Structural basis for isozyme-specific regulation of electron transfer in nitric-oxide synthase, *J. Biol. Chem. 279*, 37918.
39. Rao, P. S., and Hayon, E. (1975) Oxidation of aromatic-amines and diamines by oh radicals - formation and ionization-constants of amine cation radicals in water, *J. Phys. Chem. 79*, 1063.
40. Fujita, S., and Steenken, S. (1981) Pattern of oh radical-addition to uracil and methyl-substituted and carboxyl-substituted uracils - electron-transfer of oh adducts with n,n,n',n'-tetramethyl-para-phenylenediamine and tetranitromethane, *J. Am. Chem. Soc. 103*, 2540.
41. Hobel, B., and von Sonntag, C. (1998) Oh-radical induced degradation of ethylenediaminetetraacetic acid (edta) in aqueous solution: A pulse radiolysis study, *J. Chem. Soc. Perk. T. 2*, 509.
42. Schweizer, M., and Richter, C. (1994) Nitric-oxide potently and reversibly deenergizes mitochondria at low-oxygen tension, *Biochem. Biophys. Res. Commun. 204*, 169.
43. Devoe, I. W., and Gilchrist, J. E. (1976) Localization of tetramethylphenylenediamine-oxidase in outer cell-wall layer of neisseria-meningitidis, *J. Bacteriol. 128*, 144.
44. Marchal, S., Gorren, A. C. F., Sorlie, M., Andersson, K. K., Mayer, B., and Lange, R. (2004) Evidence of two distinct oxygen complexes of reduced endothelial nitric oxide synthase, *J. Biol. Chem. 279*, 19824.
45. Roman, L. J., and Masters, B. S. S. (2006) Electron transfer by neuronal nitric-oxide synthase is regulated by concerted interaction of calmodulin and two intrinsic regulatory elements, *J. Biol. Chem. 281*, 23111.
46. Migita, C. T., Salerno, J. C., Masters, B. S. S., Martasek, P., McMillan, K., and Ikeda-Saito, M. (1997) Substrate binding-induced changes in the epr spectra of

the ferrous nitric oxide complexes of neuronal nitric oxide synthase&#x2020, *Biochemistry 36*, 10987.

47. Huang, L., Abu-Soud, H. M., Hille, R., and Stuehr, D. J. (1999) Nitric oxide-generated p420 nitric oxide synthase: characterization and roles for tetrahydrobiopterin and substrate in protecting against or reversing the p420 conversion&#x2020, *Biochemistry 38*, 1912.
48. Sabat, J., Stuehr, D. J., Yeh, S. R., and Rousseau, D. L. (2009) Characterization of the proximal ligand in the p420 form of inducible nitric oxide synthase, *J. Am. Chem. Soc. 131*, 12186.
49. de Rosny, E., de Groot, A., Jullian-Binard, C., Borel, F., Suarez, C., Le Pape, L., Fontecilla-Camps, J. C., and Jouve, H. l. n. M. (2008) Dhr51, the drosophila melanogaster homologue of the human photoreceptor cell-specific nuclear receptor, is a thiolate heme-binding protein&#x2020, *Biochemistry 47*, 13252.
50. Raphael, A. L., and Gray, H. B. (1991) Semisynthesis of axial-ligand (position 80) mutants of cytochrome c, *J. Am. Chem. Soc. 113*, 1038.
51. Matsui, T., Nagano, S., Ishimori, K., Watanabe, Y., and Morishima, I. (1996) Preparation and reactions of myoglobin mutants bearing both proximal cysteine ligand and hydrophobic distal cavity: protein models for the active site of p-450&#x2020, *Biochemistry 35*, 13118.
52. Galinato, M. G. I., Spolitak, T., Ballou, D. P., and Lehnert, N. (2011) Elucidating the role of the proximal cysteine hydrogen-bonding network in ferric cytochrome p450cam and corresponding mutants using magnetic circular dichroism spectroscopy, *Biochemistry 50*, 1053.
53. Ueyama, N., Nishikawa, N., Yamada, Y., Okamura, T., and Nakamura, A. (1996) Cytochrome p-450 model (porphinato)(thiolato)iron(iii) complexes with single and double nh center dot center dot center dot s hydrogen bonds at the thiolate site, *J. Am. Chem. Soc. 118*, 12826.
54. Yoshioka, S., Tosha, T., Takahashi, S., Ishimori, K., Hori, H., and Morishima, I. (2002) Roles of the proximal hydrogen bonding network in cytochrome p450(cam)-catalyzed oxygenation, *J. Am. Chem. Soc. 124*, 14571.
55. Couture, M., Adak, S., Stuehr, D. J., and Rousseau, D. L. (2001) Regulation of the properties of the heme-no complexes in nitric-oxide synthase by hydrogen bonding to the proximal cysteine, *J. Biol. Chem. 276*, 38280.
56. Lang, J., Driscoll, D., Gelinas, S., Rafferty, S. P., and Couture, M. (2009) Trp180 of endothelial nos and trp56 of bacterial sanos modulate sigma bonding of the axial cysteine to the heme, *J. Inorg. Biochem. 103*, 1102.